Stony Brook University

Polymer Nanocomposites from Thermally Stable Clay

A Thesis Presented

by

Sijia Zhao

to

The Graduate School

In Partial Fulfillment of the Requirements for the Degree of

Master of Science

in

Materials Science and Engineering

Stony Brook University

August 2007

Stony Brook University

The Graduate School

Sijia Zhao

We, the thesis committee for the above candidate for the

Master of Science degree,

hereby recommend acceptance of this thesis.

Professor Miriam Rafailovich, Advisor
Department of Materials Science and Engineering

Professor Jonathan Sokolov
Department of Materials Science and Engineering

Professor Dilip Gersappe
Department of Materials Science and Engineering

This thesis is accepted by the Graduate School

Lawrence Martin
Dean of the Graduate School

Abstract of the Thesis

Polymer Nanocomposites from Thermally Stable Clay

by

Sijia Zhao

Master of Science

in

Materials Science and Engineering

Stony Brook University

2007

The thermal degradation of alkyl quaternary ammonium-modified montmorillonites limit the synthesis and processing of polymer layered silicate nanocomposites. Our efforts to address the issue focus on developing improved organophillic treatment rendering thermally stable montmorillonites. Phosphonium-containing salts were successfully employed to modify sodium montmorillonites by the standard ion exchange reaction. These organically-modified montmorillonites were characterized by thermogravimetry, Fourier transform infrared spectroscopy and small angle X-ray scattering. The use of phosphonium salts as surfactant gives the corresponding treated montmorillonites a 50-60˚C improvement in both the onset decomposition temperature and maximum weight loss temperature in nitrogen

atmosphere as compared to the commercial Cloisite® 20A. To examine the miscibility of the new clay with polymers, polystyrene (PS) resins were then compounded via melt-blending. Transmission electron microscopy and small-angle X-ray scattering results suggest that the phosphonium-treated montmorillonites were observed to be finely dispersed in the PS matrix to form a predominantly intercalated/exfoliated morphology whereas Cloisite® 20A formed micrometer-sized aggregates in PS matrix. The new surfactant appears to be more compatible with the relatively non-polar PS matrix. The nanocomposites also exhibit improved thermal and mechanical properties. Morphological evolution of the nanocomposites at progressively elevated temperature was also identified, which showed rope-like clay sheets growing in both size and length.

DEDICATION

My deepest gratitude goes to my parents, for their profound love and support throughout my life.

Table of Contents

List of Figures

List of Tables

Acknowledgement

Many people have been a part of my graduate education, as friends, teachers, and colleagues. Professor Miriam Rafailovich, first and foremost, has been all of these. I would like to express my deepest gratitude here to Professor Miriam Rafailovich. I exceptionally get inspired and enriched from her truly scientist intuition that has made her as constant oasis of ideas and passions in science. I am indebted to her more than she knows. I would like to thank my committee members Professor Jonathan Sokolov and Professor Dilip Gersappe for their suggestions and guidance throughout my study. Many thanks in particular go to Dr. Mayu Si and Professor Edward Weil for their valuable advice and constructive comments on my research. I gratefully thank Dr. Tadanori Koga for his help on the subject of small angle X-ray scattering. I was delighted to interact with Dr. Susan Vanhorn by attending her TEM training. Her insights on the subject proved to be greatly helpful. All my lab buddies at the Garcia Center made it a convivial place to work. Song Li, Yantian, Yuan Ji, Bing Quan, Xiaohua, Yuan Sun, Chunhua, Rachel, Jaseung, Jun Jiang, Zhi Pan, Xiaolan, Weiliu, Ying Liu, Seongchan, Jeffrey, Simon, Show and Tatsiana, I am fortunate to have those befriended people in my graduate study.

1. Introduction

Nanocomposites are a new class of composites that are particle-filled polymers for which at least one dimension of the dispersed particles is in the nanometer range. Depending on how many dimensions of the dispersed particles are in the nanometer range, three types of nanocomposites can be distinguished [1]. The first type is isodimensional nanoparticles, whose three dimensions are in the order of nanometers; the second type is nanotubes or whiskers where they have two dimensions in the nanometer scale and the third dimension is larger forming an elongated structure; and the last type of nanocomposites is polymer-layered crystal nanocomposites characterized by only one dimension present in the nanometer range in which case the filler forms sheets of one to a few nanometer thick to hundreds to thousands nanometers long [2-8]. Amongst all those three types of nanocomposites, polymer-layered crystal nanocomposites based on clay and layered silicates have been more widely investigated [9-10]. Their study constitutes the main subject of this thesis.

Polymer-layered silicate nanocomposites (PLSN) exhibit various superior properties such as high strength, high modulus, enhanced barrier properties, flame retardancy and ablation resistance with low weight percentages (1-5wt %) of filler content [11]. These new properties relative to conventional composites are attributed to their unique nanophase structure. Two terms (intercalated and exfoliated) are commonly used to describe the two general classes of nano-structure that can be prepared. Intercalated [1] structure is formed when a single or more extended polymer chains are intercalated between the silicate layers resulting in a well ordered multilayer morphology built up

with alternating polymeric and inorganic layers. Exfoliated [1] structure is obtained when the silicate layers are completely and uniformly dispersed in a continuous polymer matrix.

Successful formation of intercalated or exfoliated structure depends on the nature of the constituent materials (layered silicate, organic modifier and polymer matrix) and the method of preparation [1] which includes addition of layered silicates to a polymerization reaction (in situ method) [15-16]; to a solvent-swollen polymer (solution blending) [17]; or to a polymer melt (melt blending) [11, 18]. One of the most important factors influencing the nanostructure of PLSN involves the organic modification of layered silicates. Before one can give a detailed explanation of the process, we must understand the basic crystal structure of layered silicates. Layered silicates belong to the structural family known as the 2:1 phyllosilicate [11-12]. Their crystal structure consists of layers made up of two silica tetrahedral sheets fused to an edge-shared octahedral sheet of either aluminum or magnesium hydroxide. Stacking of the layer leads to a regular van der Waals gap between the layers called the interlayer or gallery. Isomorphic substitution within the layers generates charge deficiency. The deficit charges are compensated by cations (usually Na^+ or K^+) absorbed between the three-layer mineral clay [13].

A wide range of layered silicates exist in nature whereas only a few have been used in PLSN and among them the most commonly documented is montmorillonite (MMT) [33]. MMT has many advantages in that they have low cost, a high aspect ratio (100), and good swelling properties [34]. However, pristine MMT has hydrophilic interlayer surfaces that impede its homogeneous dispersion in the hydrophobic polymer matrix. Therefore, organic modification is often necessary through an ion-exchange reaction in which the organic cationic surfactants exchange with the interlayer cations. The surface energy of

thus treated layered silicates is lowered, thereby improving the wetting characteristics with the host polymer [13]. By varying the functionality, packing density and length of modifiers, the organically modified layered silicate (OLS) may be engineered to optimize the compatibility with a given polymer [14].

Long carbon-chain alkyl ammonium salts are the standard organo-treatment agents. OLS based on these modifiers prove to be applicable in low temperature resins such as polypropylene [19, 20], poly (ethylene-co-vinyl acetate) polymers [19, 21] and synthetic rubbers [19, 22]. However, when preparing nanocomposites from high-melt-temperature polymers such as polyamide-6 (PA-6), polyamide-6,6 (PA-6,6), poly(ethylene terephthalate) (PET), and polycarbonate (PC) [19], less than expected improvement in properties and in some cases, even a loss in properties was observed relative to the unfilled polymer. Davis et al [24] reported that in situ polymerized MMT/PA-6 nanocomposites (MMT treated by ammonium chloride salt of amino lauric acid) significantly degraded under injection molding conditions at 300˚C, producing a four-fold increase in ε-caprolactam content and a significant reduction in number average molecular mass, whereas virgin PA-6 did not show a decrease in number average molecular mass and only a small increase in monomer content was observed. In a separate study Davis et al [25] also observed black, brittle, and tar like MMT/PET nanocomposites produced via melt-compounding methods at 285˚C where the organic modifier is a N, N-dimethyl-N, N-dioctadecylammonium salt, indicating thermal decomposition of the nanocomposites. In a cone calorimeter evaluation of flammability property of polystyrene (PS) nanocomposites, Gilman et al [31] showed that PS melt blended with 3% dioctadecyldimethyl ammonium MMT at 185˚C has no improvement in

flammability if the extrusion condition includes high temperatures and if air is not excluded. They speculated that degradation of organic surfactant on the MMT worked in opposition to the flame retardancy mechanism of the clay.

If the processing temperature, irrespective of the fabrication route (solution mediated, in situ polymerization or melt intercalation) exceeds the thermal stability of the organic treatment on the OLS [14], degradation will occur. The organic modifier degradation could result in polymer degradation, poor clay dispersion and distribution [23]. Xie et al [14] recently conducted a detailed investigation of the thermal degradation chemistry of alkyl quaternary ammonium MMT. Their results reveal that degradation of the ammonium surfactant in the OLS proceeds by a Hoffmann elimination reaction (see Figure 1) which depends on the basicity of the anion, the steric environment around the ammonium, and temperature [14, 26]. Also relative to the parent alkyl quaternary ammonium salt, they found that the presence of catalytic sites on the aluminosilicate layer can reduce the thermal stability of a fraction of the surfactants by an average of 15-25˚C [14]. Finally, the release of organic compounds from organically modified montmorillonite is staged and is associated with retardation of product transfer arising from the morphology of the OLS [14]. Therefore, factors that influence the specific reactions and onset temperature of degradation are complex. An interplay among the source of the aluminosilicate, the anion of the ammonium salt, workup history of the organically-modified MMT, and the extent of dispersion within the polymer are recognized and not simply the size of the surfactant [26].

It was not until recently that extensive research had just begun to be devoted to the synthesis of novel thermally stable modifiers that ensure good compatibility and improve

the nanocomposite processing stability. Many ways have been proposed to offer solution to the issue. These include the use of improved purification procedures such as exhaustive extraction method [23] to completely remove anion of the ammonium salt which led to a 20˚C to 100 ˚C increase in the organically modified MMT; the use of surfactants with other cations such as pyridinium, and iminium [30] because they stand higher temperatures; approaches of untreated layered silicate in which case either the monomer [19, 27] or the curing agent [19, 28] is made cationic in situ, and this renders the layered silicate organophillic and also there is a work of applying conventional melt-compounding method furnished with an ultrasonic attachment [29] to achieve rapid intercalation and partial exfoliation without the need to chemically modify the polymer matrix.

Our own investigation of the flammability properties of high impact polystyrene (HIPS) nanocomposite system generated concern that the commercially available Cloisite series failed to withstand the high melt compounding temperature, thereby resulting in poor performance in both Underwriters Lab flammability test UL 94 and cone calorimetry test. The effectiveness of adding those Cloisite series into low processing temperature resins such as poly methyl methacrylate (PMMA) and elvacite acrylic (EVA) to enhance their thermal and flammability properties, however, has been well established as evidenced by a remarkable reduction in the heat release rate and mass loss rate from cone calorimetry. Therefore, the need is imperative to develop an organically modified MMT that endures high temperature and enables a successful preparation of polymer nanocomposites without loss of properties due to the presence of degradation products, loss of molecular mass or structural defects. In this work, we chose phosphonium

compounds to functionalize MMT and prepared nanocomposites using those clays. It is well known that phosphonium salts have been widely used as stabilizers and flame retardant agents in many applications. For example, aromatic diphenyl phosphates such as resorcinol bis (diphenyl phosphate) and bisphenol a bis (diphenyl phosphate) have broad applications in flame retardancy of polycarbonate because of their good thermal stability, high efficiency and low volatility [47]. Monophosphonium salts are widely used as heat stabilizers for nylon and stabilization agents for polyacrylonitrile fibers exposed to sunlight [26]. Therefore, phosphonium compounds if successfully applied to modify MMT may impart additional thermal and flammability properties to polymer nanocomposites.

2. Experiment

2.1 Materials

Sodium montmorillonite clay (Na^+-MMT) with a cation exchange capacity (CEC) of 92mmol/100g (mean formula unit $Na_{0.65}[Al,Fe]_4Si_8O_{20}(OH)_2$) and Cloisite® 20A (Figure 2(a)), a natural montmorillonite modified with N,N-dimethyl dihydrogenated tallow quaternary ammonium chloride (DMDTA) were provided by Southern Clay Products. DMDTA is a blend of different surfactants prepared from natural products by the Akzo Nobel Co. The major component in DMDTA was di-methy di-octadecyl-ammonia chloride (DMDOA) (>60wt%). The minor components in DMDTA are di-methyl-octaecyl-hexadecyl-ammonia chloride, di-methyl-di-hexadecyl-ammonia chloride, and a small amount (<3wt%) of tertiary ammonia chloride and di-methyl-hexadecyl-ammonia chloride [35]. Tributylhexadecyl phosphonium bromide (PC16-Br, Figure 2(b)) was purchased from Aldrich Chemical Company as a fine white solid. Polystyrene (PS) with a weight-average molecular weight (M_w): 280,000g/mol, poly-dispersity index: 1.047 and glass transition temperature (T_g): 100.0˚C was also purchased from Aldrich Chemical.

2.2 Synthesis of Ion-Exchanged Montmorillonite

The synthesis involves a cationic exchange reaction between the sodium cations of the montmorillonite clay and cations of the intercalating reagents. The equation for calculating the intercalating agent used is expressed as follows: 92/100 (CEC per 100g of the Na^+-MMT) ×5g (weight of the Na^+-MMT) ×1.2=(X/MW of the intercalating agent) ×1×1000, where 1.2 indicates the excess amount of intercalating reagent used and X, MW representing the amount and molecular weight of the intercalating reagent respectively. In a 500-ml Florence flask, a 1.7% mass fraction Na^+-MMT (5g) aqueous

suspension was agitated at 60˚C equipped with a thermometer. In a separate 250-ml Erlenmeyer flask, tributylhexadecyl phosphonium bromide (2.82g) was dissolved in a 50:50 mixture of ethanol and deionized H_2O at 60˚C. This was then added to the heated Na^+-MMT suspension and a white precipitate was immediately seen. However, the reaction mixture was stirred for an additional 8h under the same mixing conditions.

PC16-MMT was collected by filtration using a Buchner funnel, Whatman #5 filter paper and low vacuum and subsequently washed with a combination of 50:50 hot ethanol and deionized H_2O. $AgNO_3$ was used to test the absence of bromide anions. The filter cake was dried at room temperature, grounded with a mortar and pestle and further dried under vacuum at 100˚C overnight.

2.3 Preparation of Polystyrene-Layered-Silicate Nanocomposites

PS and organically modified MMT were dried overnight in a vacuum oven at 100˚C before processing. PS nanocomposites were prepared by melt compounding in a C.W. Brabender operating at 185˚C. A total of 50g was divided into the calculated weight ratios of PS (95%) and Na^+-MMT (5%), Cloisite® 20A (5%) or PC16-MMT (5%), respectively. In order to obtain thorough mixing, PS polymer was first inserted into the chamber and mixed at 20 rpm for 1 min. The different clays were then added and mixed at 100 rpm for 15 min. The samples were molded into various shapes in a hot press for the following characterization techniques.

2.4 Thermogravimetric Analysis Measurements

Thermogravimetric analysis (TGA) was conducted on a NETZSCH STA 449C instrument under nitrogen atmosphere, heated from room temperature to 800˚C at a rate of 10˚C/min. Individual samples with weight between 5-10mg are placed into a crucible

pan attached to a sensitive microbalance assembly. The sample holder portion of the TGA balance assembly is then placed into a high temperature furnace. The balance assembly measures the initial sample weight at room temperature and then continuously monitors changes in sample weight as heating rate increases. Weight loss profiles are analyzed for the amount or percent of weight loss at any given temperature, the amount or percent of non-combusted residue at some final temperature, and the temperatures of various sample degradation processes.

2.5 Fourier Transform Infrared Spectroscopy

Fourier transform infrared spectroscopy (FTIR) spectra were collected using a Nicolet MAGNA-IR 760 spectrometer by the standard KBr disk method in the range of 650-4000 cm^{-1} with a nominal resolution of $4cm^{-1}$.

2.6 Small Angle X-ray Scattering Measurements

Small angle X-ray scattering (SAXS) measurements were performed at the X10A beamline of the National Synchrotron Light Source (NSLS) at Brookhaven National Laboratory. The wavelength of the X-ray beam was 0.11nm. The sample-to-detector distance was about 500mm. An imaging plate was used for pattern detection.

2.7 Transmission Electron Microscopy

Bright field transmission electron microscopy (TEM) images of PS nanocomposites were obtained at 80kV with a JEOL JEM1200ex electron microscope. Cross sections about 70nm thick of the sample were ultramicrotomed with a diamond knife at room temperature using a Reichert-Jung Ultracut E microtome. The ultrathin films were then floated from water onto copper grids. Since the contrast between the polymer phase and layered silicate sufficed for imaging, heavy metal staining of sections is not required [31].

2.8 Dynamical Mechanical Analysis Measurements

Dynamical mechanical properties were investigated using a Mettler Toledo DMA/SDTA861e dynamic mechanical analyzer (DMA) in a single cantilever bend mode. Molded samples with a dimension of $10\times10\times2mm^3$ were measured from room temperature to 200˚C at a constant frequency of 1Hz and a heating rate of 2˚C/min.

3. Results and Discussion

3.1 Organically-Modified Montmorillonite

MMT was organically treated with an aliphatic (PC16-Br) phosphonium salt. For comparison purpose, a conventional quaternary ammonium salt modified MMT (Cloisite® 20A) was also evaluated. The results of TGA analysis recorded under nitrogen atmosphere are summarized in table 1. The onset decomposition temperature as commonly defined in literature [25] on the basis of a 5% weight loss of the initial host MMT for PC16-MMT is evidently higher than that of the Cloisite® 20A. In addition, the peak decomposition temperature corresponding to the maximum weight loss of the phosphonium based MMTs shift to higher regions compared to the commercial Cloisite® 20A. The organic content can be determined by adjusting the total mass loss up to 800˚C with the mass loss of the parent Na^+-MMT involving the dehydroxylation of the aluminosilicate [26].

Figure 1 shows the derivative thermogravimetry (DTG) curves of decomposition profile for Na^+-MMT and Cloisite® 20A. A first event of weight loss was clearly observed for Na^+-MMT at around 84˚C which identifies region I (below 180˚C) to account for the evolution of physically absorbed water and gaseous species. Region II (200-500˚C) is characteristic of Cloisite® 20A where organic substances evolve. In region III (500-700˚C) dehydroxylation of the aluminosilicate occurs. Finally, region IV (700-1000˚C) is associated with the evolution of residual organic carbonaceous residue which is absent in Na^+-MMT. The above convenient "four regions" consideration of decomposition profile for organically-modified MMT is well documented [14].

A further look at the decomposition profile of PC16-MMT as shown in Figure 2 reveals a similar trend except where region II expands toward a higher temperature regime, indicating an advantageous thermal stability over Cloisite® 20A. Region I and II is an important service environment for nanocomposite fabrication because the release of small molecules from MMT or the evolution of decomposition products may potentially affect the interface between the polymer matrix and silicate [26].

Figure 3 depicts the SAXS profile for Na^+-MMT, Cloisite® 20A and PC16-MMT respectively, where the plots are arbitrarily shifted for comparison purposes. The scattering vector q is defined as $4\pi\sin\theta/\lambda$. The PC16-MMT curve shows a first order strong peak at $q=0.2516Å^{-1}$ and a second order peak at around $q=0.5030Å^{-1}$ which is roughly twice the distance of the first peak position. The d-spacing or gallery spacing change corresponding to the [001] direction between MMT sheets upon organic treatment was determined by SAXS using the formula $d_{001}=2\pi/q$. Results suggest an increase of gallery spacing to 25.0Å for PC16-MMT compared to only 11.7Å for pristine Na^+-MMT. Larger gallery spacing normally helps translate into enhanced dispersion and delamination in the polymer [25]. On the other hand, the two characteristic SAXS maxima of Cloisite® 20A are observed in slightly lower q regions where the d_{001} spacing of the clay is calculated to be 27.6Å. It is also worthwhile to notice the much broader peak shape of Cloitsite 20A in contrast with the pronounced sharp and narrow ones of PC16-MMT. Broader peak generally indicates a multimodal distribution of the d-spacing in the clay. Since Cloisite® 20A has more surfactant content than PC16-MMT as the TGA calculation clearly showed, it is possible that there still exist galleries that are not interchanged with the phosphonium salts and retain the pristine spacing of Na^+-MMT.

Figure 4 shows the FTIR spectra of Na^+-MMT, PC16-Br and PC16-MMT whereas tentative assignments of the infrared bands corresponding to each species were illustrated in Table 2. The absorption bands at 1040, 1630 and 3620cm^{-1} are characteristic of pristine Na^+-MMT. The very strong infrared absorption bands at 1040cm^{-1} are due to Si-O stretching vibrations of montmorillonite. The weak band at 1630cm^{-1} is ascribed to the stretching and deformation vibrations of the water molecules residing in between the Na^+-MMT gallery. The strong one at 3620cm^{-1} results from the -OH group stretching vibration of the Na^+-MMT. The curve for PC16-Br has characteristic bands at 1460, 2850, and 2920cm^{-1}. The occurrence of very strong absorption at 2850 and 2920cm^{-1} for the salt is due to the C-H symmetric stretching and C-H asymmetric stretching of PC16-Br while the stretching of C-P group may lead to the peak at 1460cm^{-1} [36]. Now looking at the spectra of PC16-MMT which were synthesized via the ion-exchanged reaction between Na^+-MMT and PC16-Br, it is evident that it preserved the important characteristic bands of both the parent constituent. The difference lies in the diminished intensity of the absorption bands possibly due to the fact that the concentrations of both PC16-Br and Na^+-MMT in the resultant PC16-MMT are less compared to the pure samples. The additional difference worthy to point out is that the 1630cm^{-1} band otherwise present in the pristine Na^+-MMT disappeared. The reason finds straightforward explanation in the annealing experiment at 100˚C that was conducted for PC16-MMT before its characterization. This step essentially helped to remove the weakly-bound interlayer water molecules in the montmorillonite, thereby ensuring valid interpretation for TGA data and stable melt processing condition.

3.2 Morphology of Polystyrene-Layered-Silicate Nanocomposites by TEM & SAXS

Although the thermal stability of organically-modified MMT is of critical importance in fabricating polymer-layered-silicate nanocomposite, the functionality on the MMT must also be compatible with the polymeric matrix in order to render itself well dispersed, thus forming a nanocomposite instead of an immiscible conventional composite [19]. Toward this end, we studied the morphology of PS blended with PC16-MMT (5% mass fraction) in a Brabender at 185˚C under 10min residence time. Two control samples, PS/Na^+-MMT and PS/Cloisite® 20A processed under the same conditions were also thoroughly investigated. TEM images showing varying degrees of dispersion were provided in Figure 5. For the PS/PC16-MMT samples, the low magnification TEM image (Figure 5 (c)) showed the clay to be finely dispersed throughout the polymer, forming an orientation that parallels the shear direction during polymer processing. Small tactoids were predominantly present whereas sparsely scattered large tactoids did also appear. Higher magnification TEM image (Figure 5 (d)) showed regions where both intercalated and exfoliated structures existed and regions where both intercalated tactoids and a few individual layers were present. However, TEM analysis of both PS/Na^+-MMT and PS/Cloisite® 20A (Figure 5 (a), (b)) showed very large and unevenly dispersed big tactoids observed at low magnification, suggesting an immiscible dispersion.

To further confirm the qualitative results obtained by TEM, SAXS measurements were carried out as a complementary technique to describe the morphology of the materials. Figure 6 shows both the SAXS profile for pure PC16-MMT and PS/PC16-MMT samples. The two strong and sharp scattering peaks present in PC16-MMT suggest ordered clay sheets stacked together. In contrast, the curve of PS/PC16-MMT exhibits

only a first order maximum with much reduced scattering intensity and broadened peak. This indicates that the clay sheets had been disturbed to break down into smaller numbers per crystallite due to the strong shear generated by the Brabender. The broadness of the peak might suggest that a diversity of structures existed [33] and also come from possible local clay disorder. This interpretation is consistent with the TEM images of partially intercalated and exfoliated PS/PC16-MMT system. The results of the SAXS profile for pure Cloisite® 20A and PS/Cloisite® 20A are illustrated in Figure 7. The shape of the SAXS profile for PS/Cloisite® 20A is similar to the profile of pure Cloisite® 20A; however, the peak's position shifted to lower q regions. The presence of two distinct peaks with the second one twice the distance of the first peak is a sign of well-stacked clay structure usually containing multiple sheets. The movement of peak positions into lower q values which correspond to larger gallery spacing suggests polymer chains penetrated into the interlayer between clay sheets but provides limited information as to what extent the intercalation occurred. TEM images of PS/Cloisite® 20A showed the morphology largely remains phase-separated.

3.3 Viscoelastic Properties of Polystyrene-Layered-Silicate Nanocomposites

Dynamic mechanical analysis for the PS/MMT nanocomposites was carried out to study the effect of clay on their thermo-mechanical properties. The temperature dependence of storage modulus (E') and tan δ are plotted in Figures 10 and 11, respectively. Examination of the storage modulus plots reveals that the addition of 5% PC16-MMT into PS matrix produces a remarkable enhancement in the stiffness of the material. The E' curve before the glass transition temperature (T_g) roughly exhibits an 30% increase over the pure PS and above the T_g in the rubbery state, the stiffness of the material is also well maintained with values slightly higher than that of the pure PS polymer. The addition of inorganic fillers like clay generally induces reinforcement effect. For clay, in particular, a proposed mechanism of reinforcement is due to its large aspect ratio of the structural hierarchy in the nano-scale level which restricts segmental motion near the organic inorganic interface [38, 39] and possibly also comes from the polymer chain which interacts with the large surface areas of the clay again preventing its motion. In recognizing the property enhancement attributes from adding clay, we have assumed two factors governing the performance, the extent of dispersion and interaction of clay particles with polymer matrix. In contrast, PS/Cloisite® 20A with the same clay content showed almost little improvement in its modulus below T_g and appears to lose much of its stiffness in the rubbery plateau. The possible explanation might be the fact that aggregated Cloisite® 20A particles in PS matrix fails to produce a strong physical block restricting the motion of polymer chains.

In Figure 11 the plot of tan δ as a function of temperature shows a reduction in the intensities of the peaks for PS/PC16-MMT and PS/Cloisite® 20A while almost no change

can be observed for their shapes and positions. The curves for PS/Na^+-MMT is almost identical with the pure PS. Tan δ, equal to the ratio between the loss modulus (E'') and the storage modulus (E') is a measurement of relaxation process for the polymer. The decrease in the height of tan δ might be explained in terms of the restricted mobility for the polymer chains. However, it might not be enough to significantly affect the transition temperature of the material [40]. Therefore, the peak position of tan δ corresponding to the glass transition temperature for the PS/PC16-MMT and PS/Cloisite® 20A nanocomposites remain almost unchanged relative to the amorphous virgin PS.

3.4 Thermal Stability of Polystyrene-Layered-Silicate Nanocomposites

The organic modifier used to functionalize the clay surface can be quite volatile, and hence conventionally, there is some controversy as to the flame retardant benefits of adding these clays in composite materials [43]. Any changes in the thermal property of PS nanocomposite by employing the new phosphonium-based MMT with 50-60˚C higher decomposition temperature in this work deserve careful investigations. The TGA curves for PS, PS/Cloisite® 20A and PS/PC16-MMT nanocomposites under nitrogen flow are shown in Figure 12. The onset thermal degradation temperatures of both PS/Cloisite® 20A and PS/PC16-MMT overlap and are comparable with the virgin polymer, showing little signs of improvement. Indeed, it has already been found that the addition of clay into PP matrix can catalyze its initial decomposition and leads to the shortening of ignition time [41, 42]. This phenomenon was attributed to the early decomposition of the ammonium organic modifier which causes a quick release of fuel in the ignition process [44].

However, the 50% degradation temperature was improved compared to the pure PS polymer which suggests the volatilization rate is impeded in both PS/Cloisite® 20A and PS/PC16-MMT. The charring effect significantly increased for the PS/PC16-MMT nanocomposites during the period. At even higher temperature, the weights of the final residue of both samples at 600˚C were found to increase by 4-5%. The formation of chars in nanocomposites is usually considered to be the dominating view for enhanced thermal stability because they supposedly hinder the diffusion of the volatile degradation products and limit oxygen inflow [45] and also act as barrier to heat and mass transport inside the bulk nanocomposite material [46].

A close look at the TGA curve for the phosphonium-containing nanocomposite revealed two steps reaction in the degradation pathway, which finds no presence in the other two materials. The same phenomenon, observed by Zhu et al [37] also occurred when an n-hexadecyl triphenylphosphonium-modified MMT was polymerized with styrene monomer to make the nanocomposite.

TGA provides a quantitative sample weight loss profile as a function of programmed heating rate. It would also be interesting to examine nanocomposite morphological changes as temperature increases. As an attempt to gain more insight to the thermal properties of nanocomposite, PC/16-MMT nanocomposites samples were heated in a ceramic oven in a 50˚C stepwise increase manner while maintaining each temperature for 5 min. Samples from each annealing step were removed and analyzed. Thin cross sections of about 70-80nm from each annealed sample were obtained using an ultra-microtome for TEM analysis. Figure 13 shows the TEM images of PC/16-MMT nanocomposites at room temperature, 250˚C, 300˚C and 350˚C. When temperature reaches 250˚C, clay sheets appear to relax and lose the orientation structure induced by the shear during melt compounding. As the temperature was raised to 300˚C, some of the clay sheets seem to self-assemble into thick and long rope-like structures with a diminished degree of exfoliation. The collapse of intercalated/exfoliated clay sheets is due to the dissociation of the organic surfactant from their surfaces. A further increase in temperature to 350˚C led to a similar morphology compared to the 300˚C image. Randomly dispersed clay sheets are present in various forms. When temperature goes beyond 400˚C, cross sectioning of the materials becomes hard because the PS matrix degraded severely.

4. Conclusion

A tributylhexadecyl phosphonium bromide (PC16-Br) salt was ion-exchanged with pristine Na^+-MMT to obtain a novel organically modified MMT which achieved an improved thermal stability over its conventional quaternary ammonium modified MMT counterpart. An increase of 50˚C-60˚C in both the onset decomposition temperature and maximum weight loss temperature was observed from TGA analysis. Hoffman elimination reaction believed to be the degradation mechanism in the conventional quaternary ammonium modified MMT was likely to be rendered difficult with the new phosphonium PC16-MMT. SAXS measurements revealed that PC16-MMT has an expanded gallery spacing of 25Å. Big interlayer spacing facilitates polymer intercalation. When 5% (mass fraction) PC16-MMT was melt blended with PS, a partially intercalated/exfoliated nanocomposite is formed as confirmed by TEM and SAXS. This suggests that a good interaction exists between the relatively non-polar backbone of PS matrix and the surfactant on the surface of PC16-MMT. The nanocomposite exhibits improved storage modulus by a factor of 30% at room temperature. Enhanced thermal stability and char yield were also observed compared to the virgin PS polymer.

5. Future Work

The introduction of clay into polymer has been shown to impart the nanocomposites flame retardant properties, namely a significant decrease in the peak release rate, a change in the char structure, and a decrease in the rate of mass loss during combustion in a cone calorimeter. However, adding clay alone does not guarantee to pass the industrially-significant Underwriters Lab test UL94 standard. Polymer nanocomposites perform poorly with respect to extinction time. Dr. Mayu Si [43] of our group has demonstrated the synergism between conventional flame retardants and organoclay in PMMA. He found that PMMA with both the above components passed the UL 94 V0 test and organoclay effectively improves the dispersion of flame retardant agents while at the same time the needed amount is greatly reduced.

An area of interest worth to be investigated is to melt-blend high temperature resins such as HIPS and PC with the novel thermally stable PC16-MMT and conventional flame retardant agents. The new clay might provide an alternative to enhance fire performance of these materials.

6. Reference

1. Michael, A.; Philippe, D. *Materials Science and Engineering* 2000, 2, 28.
2. Mark, J.E.; *Polym. Eng. Sci.* 1996, 36, 2905-2920
3. Reynaud, E.; Gauthier, C.; Perez, J.; *Rev. Metall./Cah. Inf. Tech.* 1999, 96, 169-176
4. Von Werne, T.; Patten, T.E.; *J. Am. Chem. Soc.* 1999, 121, 7409-7410
5. Herron, N.; Thron, D.L.; *Adv. Mater.* 1998, 10, 1173-1184
6. Calvert, P.; Potential applications of nanotubes, in: T.W. Ebbesen (Ed.), Carbon Nanotubes, *CRC Press, Boca Raton,* FL, 1997, pp.277-292
7. Favier, V.; Canova, G.R.; Shrivastava, S.C.; Cavaille, J.Y.; *Polym. Eng. Sci.* 1997, 37, 1732-1739
8. Chazeau, L.; Cavaille, J.Y.; Canova, G.; Dendievel, R.; Boutherin, B.; *J. Appl. Polym. Sci.* 1999, 71, 1797-1808
9. Theng, B.K.G.; The Chemistry of Clay-Organic Reactions, *Wiley*, New York, 1974
10. Ogawa, M.; Kuroda, K.; *Bull. Chem. Soc. Jpn*. 1997, 70, 2593-2618
11. Giannelis, E.P.; *Adv. Mater.* 1996, 8, 29
12. Brindely, G.W.; Brown, G.; Crystal Structure of Clay Minerals and Their X-ray Identification, *Mineralogical Society*, London, 1980
13. Awad, W.H.; Gilman, J.W.; Nyden, M.; Harris, R.H., Jr.; *Thermochimica Acta.* 2004, 409, 3-11
14. Xie, W.; Gao, Z.; Pan, W-P.; *Chem. Mater.* 2001, 13, 2979-2990
15. Lan, T.; Pinnavaia, T.J. *Chem. Mater.* 1994, 6, 2216
16. Usuki, A.; Kojima, Y.; Kawasumi, M.; Okada, A.; Fukushima, Y.; Kurauchi, T.; Kamigaito, O. *J. Mater. Res.* 1993, 8, 1179

17. Jeon, H. G.; Jung, H.T.; Lee, S. D.; Hudson, S. *Polymer Bulletin* 1998, 41, 107
18. Fisher, H.; Gielgen, L.; Koster, T. Nanocomposites from Poly-mersand Layered Minerals; TNO-TPD Report, 1998
19. Gilman, J.W.; Awad, W.H.; Davis, R.D.; Shields, J.; Harris, R.H. Jr., Davis, C.; *Chem. Mater.* 2002, 14, 3776-3785
20. 2002 GMC Safari and Chevrolet Astro vans. Step assist. See: http://www.nanoclay.com/news.html
21. Sud-Chemie/Kabelwerk Eupen; 2000, Flameproof Polymer Composition. PCT Application WO 00/68312, 2000. Beyer, G. In Flame Retardants 2002, Interscience Communications: London, 2002; pp 209-216
22. Wilson/InMat Double Core tennis balls. See: http://www.inmat.com
23. Davis, R.D.; Gilman, J.W.; *Clays and Clay Minerals* 2004, Vol.52, 2, 171-179
24. Davis, R.D.; Gilman, J.W.; *Polymer Degradation and Stability* 2003, 79, 111-121
25. Davis, C.H.; *Journal of Polymer Science: Part B: Polymer Physics* 2002, 40, 2661-2666
26. Xie, W.; Xie, R.; Pan, W.P.; *Chem. Mater.* 2002, 14, 4837-4845
27. Yasue, K.; Tamura, T.; Kathahira, S.; Watanabe, M. (Unitika Ltd.). U.S. Patent 5,414,042, 1995
28. Pinnavaia, T.; Lan, T. (Claytech Inc.). U.S. Patent 5, 853, 886, 1998
29. Lapshin, S.; Isayev, A.I.; *Journal of Vinyl & Additive Technology* 2006, 12, 78-82
30. Takekoshi, T.; Khouri, F. F.; Campbell, J.R.; Jordan, T.C.; Dai, K.H. (General Electric Company). U.S. Patent 5,707,439, 1998

31. Gilman, J.W.; Jackson, C.L.; Morgan, A.B.; Harris Jr., R.; *Chem. Mater.* 2000, 12, 1866-1873
32. See: http://www.scprod.com/product_bulletins/PB%20Cloisite%20NA+.pdf
33. Morgan, A.B.; Gilman, J.W.; *Journal of Applied Polymer Science* 2003, 87, 1329-1338
34. Vermogen, A.; Varlot, K.M.; Séguéla R.; *Macromolecules* 2005, 38, 9661-9669
35. Gelfer, M.Y.; Song, H.H.; Liu, L.Z.; Hsiao, B.S.; Chu, B.; Rafailovich, M.; Si, M.Y.; Zaitsev, V.; *Journal of Polymer Science: Part B: Polymer Physics* 2003, 41, 44-54
36. Chen, G.M.; Liu, S.H.; Chen, S.J.; Qi, Z.N.; *Macromol. Chem. Phys.* 2001, 202, 1189-1193
37. Zhu, J.; Morgan, A.B.; Lamelas, F.J.; Wilkie, C.A.; *Chem. Mater.* 2001, 13, 3774-3780
38. Agag, T.; Koga, T.; Takeichi, T.; *Polymer* 2000, 42, 3399-3408
39. Agag, A.; Takeichi T.; *Polymer* 2000, 41, 7083
40. Shi, Y.; Peterson, S.; Sogah, D.Y.; *Chem. Mater.* 2007, 19, 1552-1564
41. Qin, H.L.; Su, Q.S., Zhang S.M.; Zhao, B.; Yang, M.S.; *Polymer* 2003, 44, 7533
42. Qin, H.L.; Zhang, S.M., Zhao, C.G.; Feng, M., Yang M.S.; Shu, Z.J.; *Polym Degrad Stab.* 2004, 85, 807
43. Si, M.Y.; Polymer Nanocomposites with Enhanced Thermal and Mechanical Properties; *Dissertation*, 2006
44. Morgan, A.B.; Chu, L.L.; Harris J.D.; *Fire Mater.* 2005; 29, 213-229
45. Leszczyńska, A.; Njuguna, J.; Pielichowski, K.; Banerjee, J.R.; *Thermochimica Acta* 2007, 453, 75-96

46. Leszczyńska, A.; Njuguna, J.; Pielichowski, K.; Banerjee, J.R.; *Thermochimica Acta* 2007, 454, 1-22

47. Levchik, A.V.; Weil, E.D.; Progress in Phosphorous-based Flame Retardants; IPMEC Conference, Sept.19, 2005, Shanghai

Table 1: Property and thermal stability data (TGA) for organically-modified MMTs

sample	milliequivalent exchange ratio MER per 100g	organic fraction (%)	onset decomposition temp (˚C)	peak decomposition temp (˚C)	gallery spacing (Å)
Na^+-MMT	92.6	N/A	N/A	N/A	11.7
Cloisite® 20A	95	31.11	301	392	27.6
PC16-MMT	92.6	23.20	362	442	25.0

Table 2: FTIR band assignments of pristine MMT (Na^+-MMT) and tributylhexadecyl phosphonium modified MMT (PC16-MMT) [36]

frequency^{-1} (cm)	intensity	tentative assignment
1040	very strong	Si-O stretching
1460	medium	C-P stretching
1630	weak	interlayer H_2O deformation
2850	strong	C-H symmetric stretching
2920	strong	C-H asymmetric stretching
3620	medium	-OH stretching

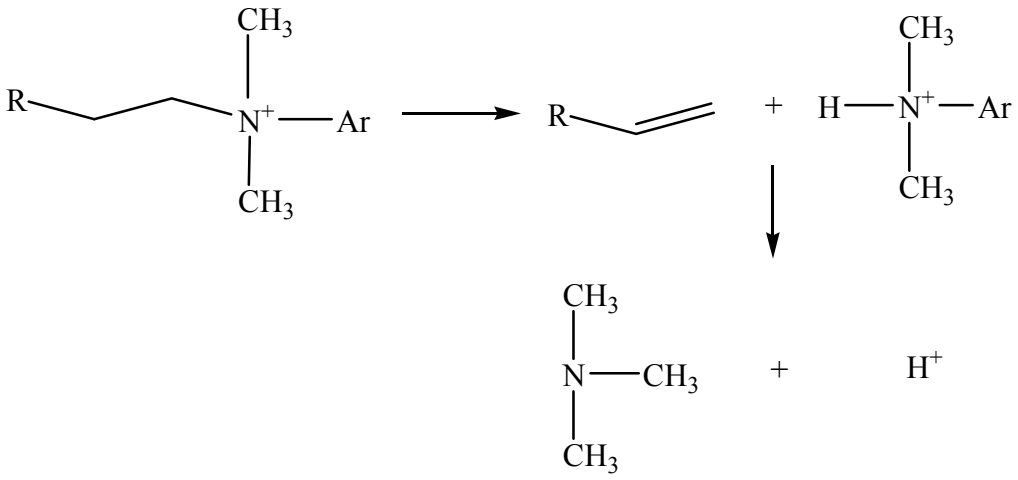

Figure 1: Thermal degradation chemistry of alkyl quaternary ammonium MMT producing an olefin and an amine while leaving a proton occupying the cationic position on the clay [37]

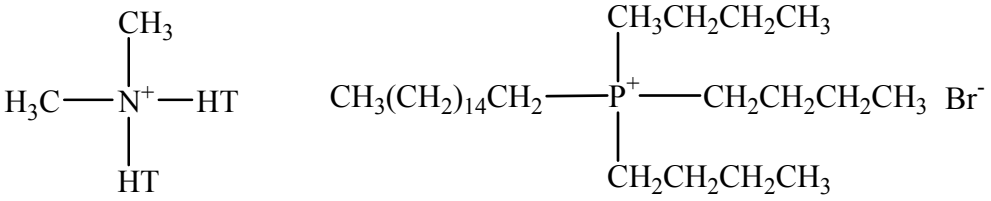

(a) (b)

Figure 2: Structure of (a) Cloisite® 20A where HT is Hydrogenated Tallow (~65% C18; ~30% C16; ~15% C14), and (b) tributylhexadecyl phosphonium bromide (PC16-Br) used to organically modify pristine Na^+-MMT

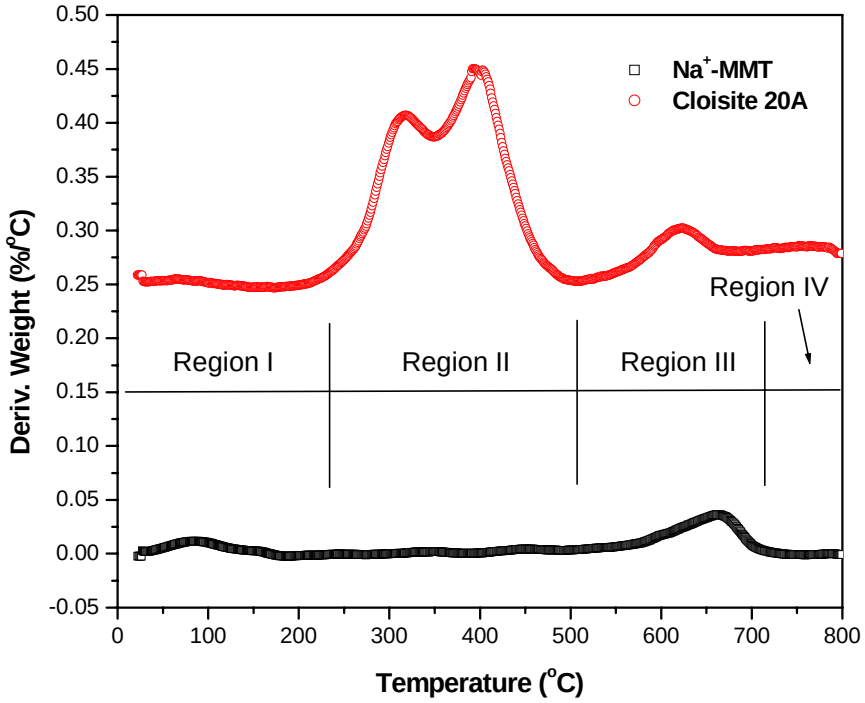

Figure 3: Derivative weight loss (DTG) curves comparing N, N-dimethyl dihydrogenated tallow quaternary ammonium modified MMT (Cloisite® 20A) and pristine MMT (Na^+-MMT)

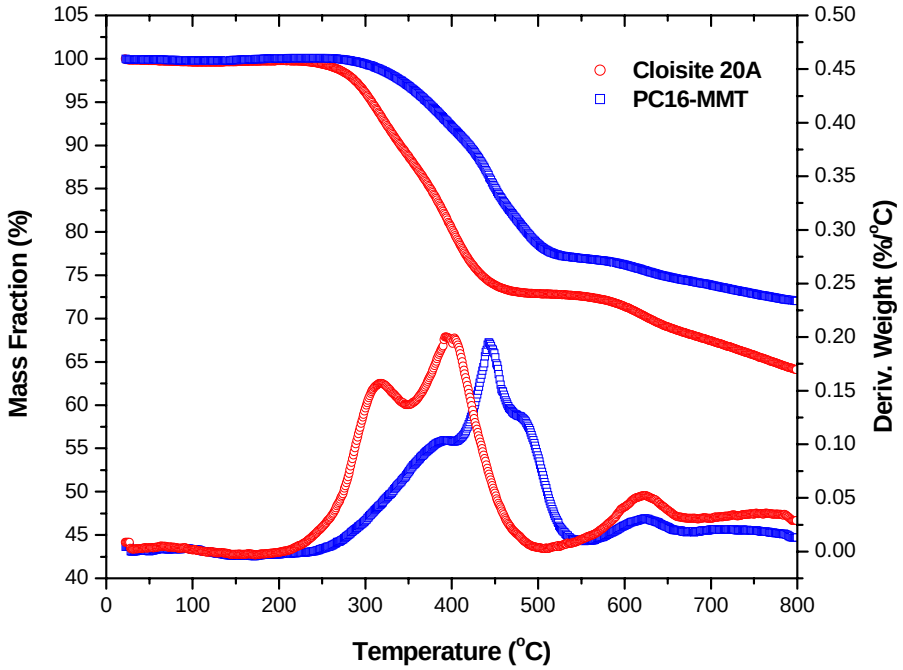

Figure 4: TGA data for N, N-dimethyl dihydrogenated tallow quaternary ammonium modified MMT (Cloisite® 20A) and tributylhexadecyl phosphonium modified MMT (PC16-MMT)

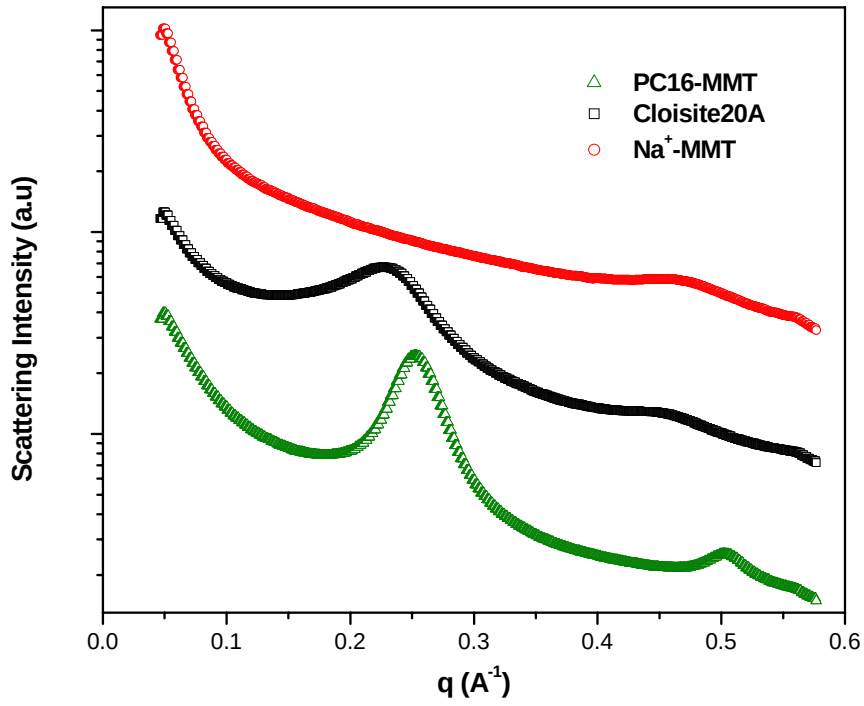

Figure 5: SAXS profiles of pristine MMT (Na^+-MMT), N, N-dimethyl dihydrogenated tallow quaternary ammonium modified MMT (Cloisite® 20A) and tributylhexadecyl phosphonium modified MMT (PC16-MMT)

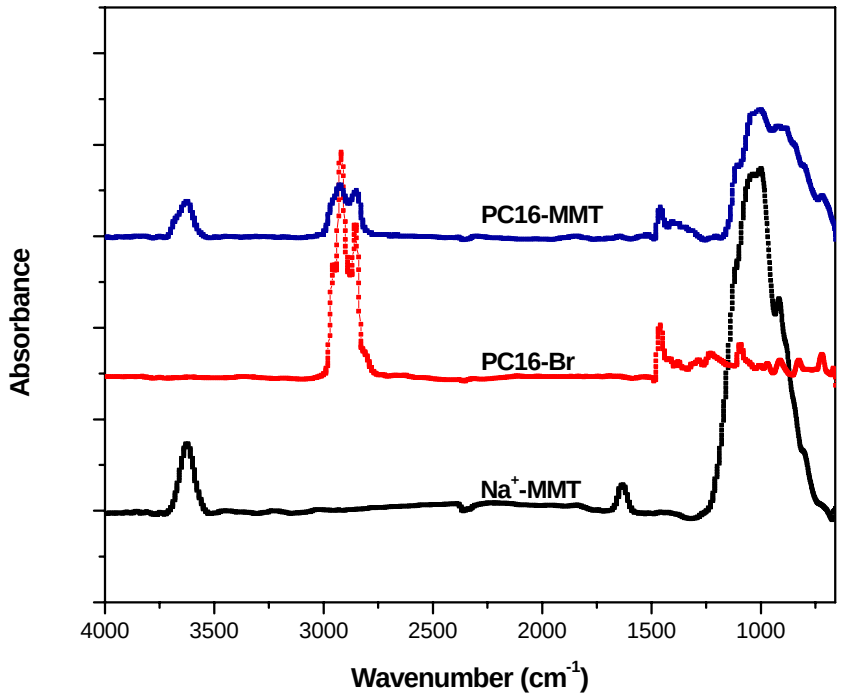

Figure 6: FT-IR spectra of pristine MMT (Na^+-MMT), tributylhexadecyl phosphonium bromide (PC16-Br) and tributylhexadecyl phosphonium modified MMT (PC16-MMT)

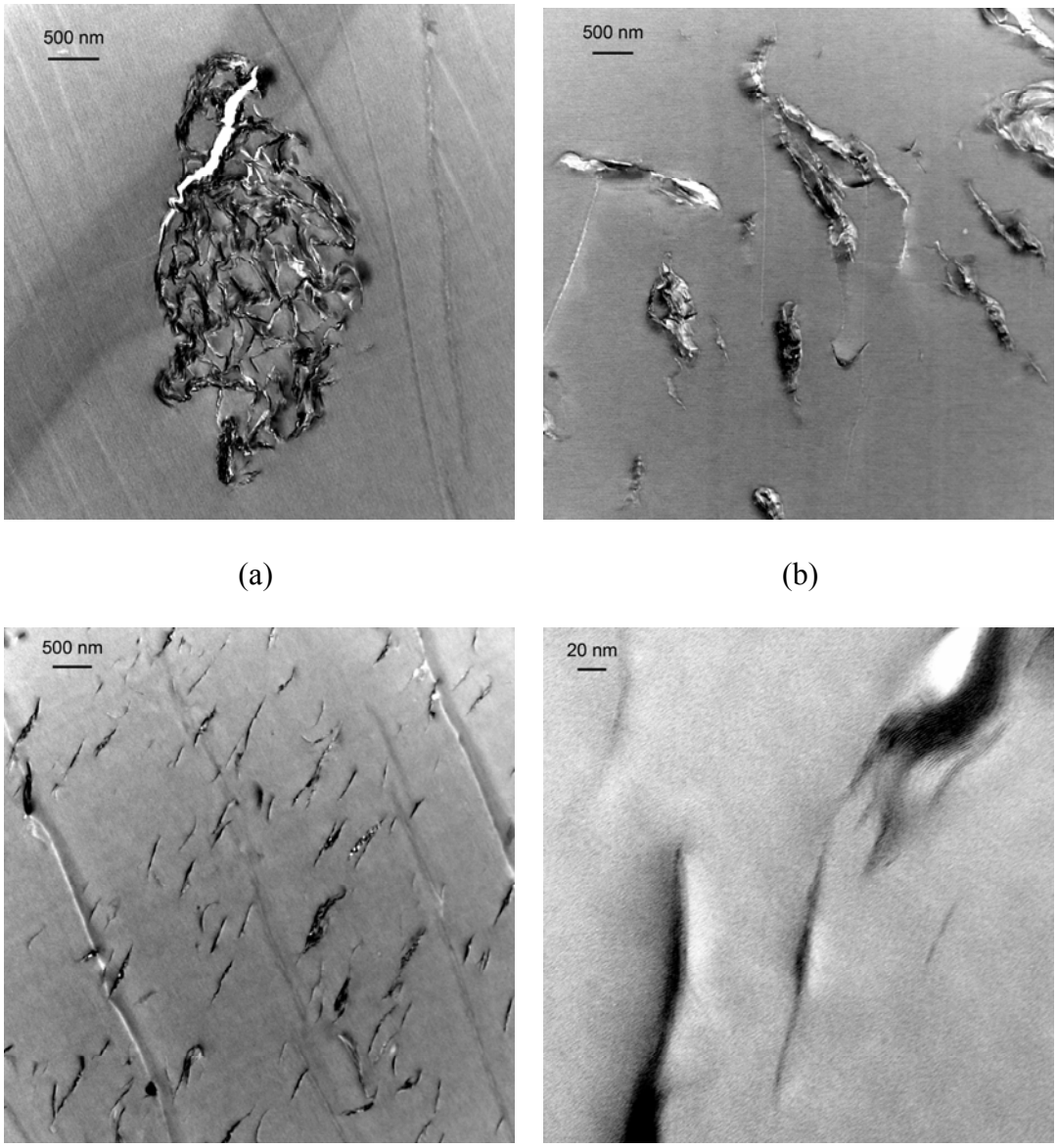

(a) (b)

(c) (d)

Figure 7: Low magnification TEM image of: (a) an immiscible Na^{+}-MMT/PS nanocomposite (5% mass fraction), (b) an immiscible Cloisite® 20A/PS nanocomposite (5% mass fraction), (c) an intercalated/exfoliated PC16-MMT/PS nanocomposite (5% mass fraction); High magnification TEM image of : (d) an intercalated/exfoliated PC16-MMT/PS nanocomposite (5% mass fraction)

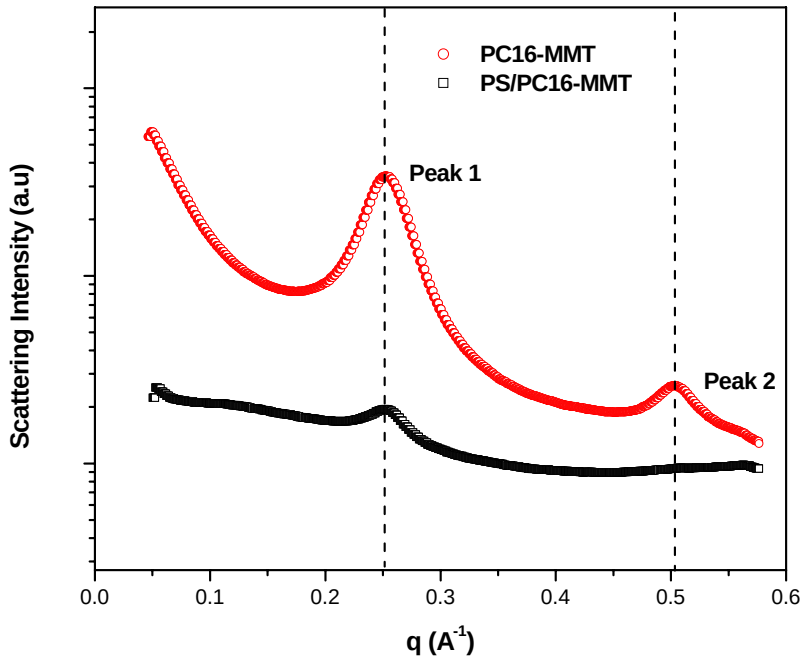

Figure 8: SAXS profiles of pure tributylhexadecyl phosphonium modified MMT (PC16-MMT) and PC16-MMT/PS nanocomposite (5% mass fraction)

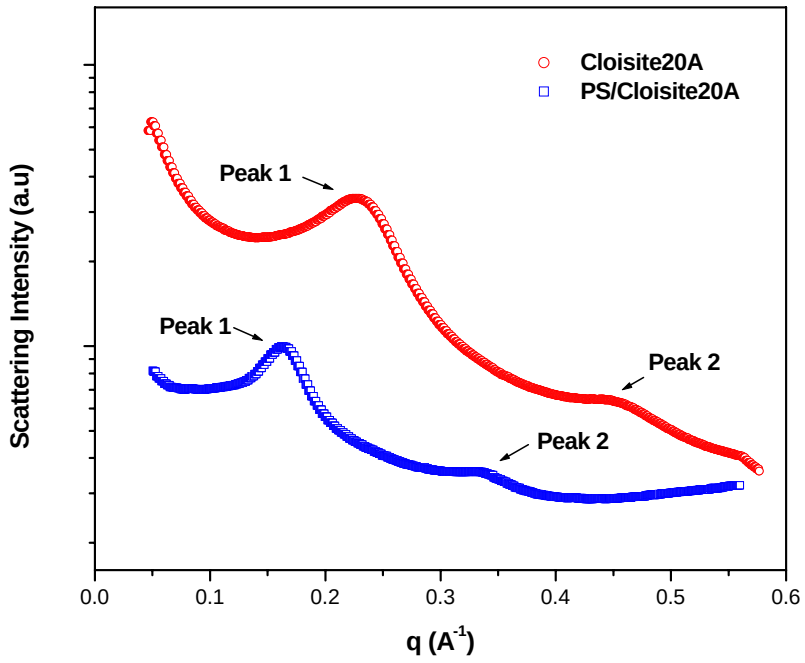

Figure 9: SAXS profiles of pure N, N-dimethyl dihydrogenated tallow quaternary ammonium modified MMT (Cloisite® 20A) and PC16-MMT/PS nanocomposite (5% mass fraction)

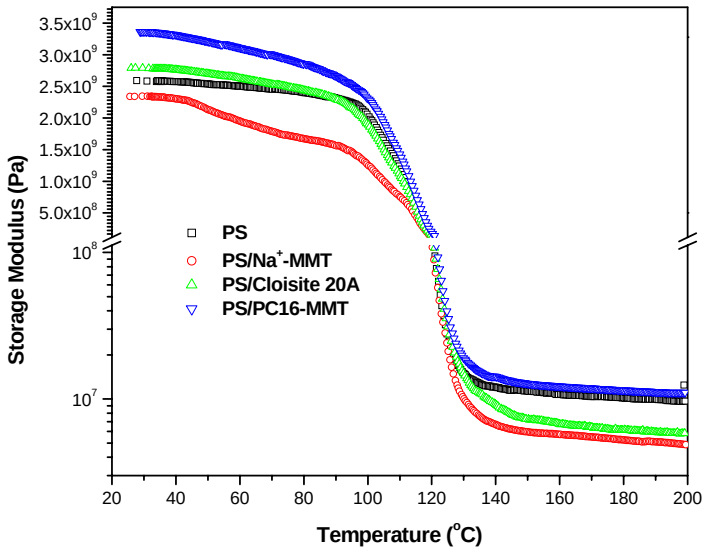

Figure 10: Storage modulus versus temperature curves of pure PS; PS/Na^+-MMT nanocomposite (5% mass fraction), PS/ Cloisite® 20A nanocomposite (5% mass fraction), and PS/PC16-MMT nanocomposite (5% mass fraction)

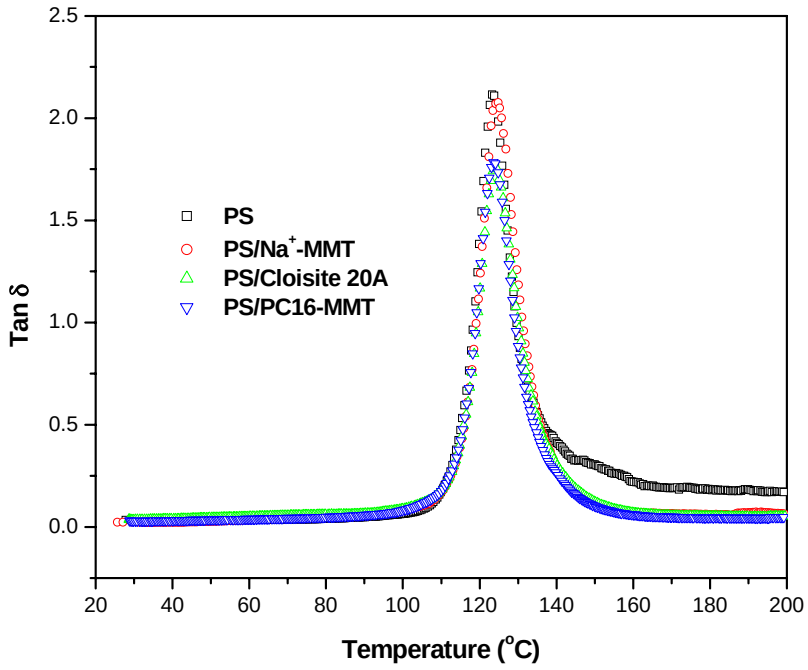

Figure 11: Tan δ versus temperature curves of pure PS; PS/Na^+-MMT nanocomposite (5% mass fraction), PS/ Cloisite® 20A nanocomposite (5% mass fraction), and PS/PC16-MMT nanocomposite (5% mass fraction)

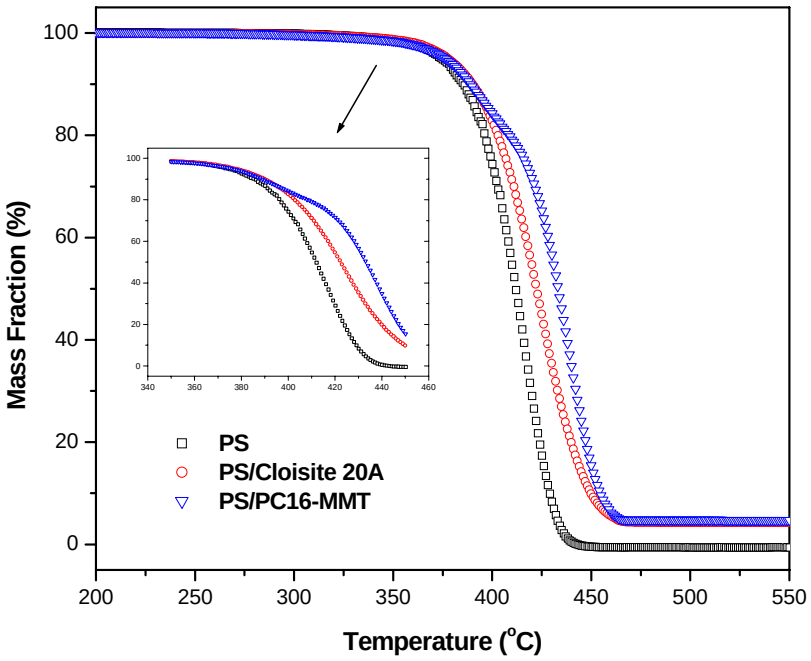

Figure 12: TGA curves for pure PS, PS/ Cloisite® 20A nanocomposite (5% mass fraction), and PS/PC16-MMT nanocomposite (5% mass fraction)

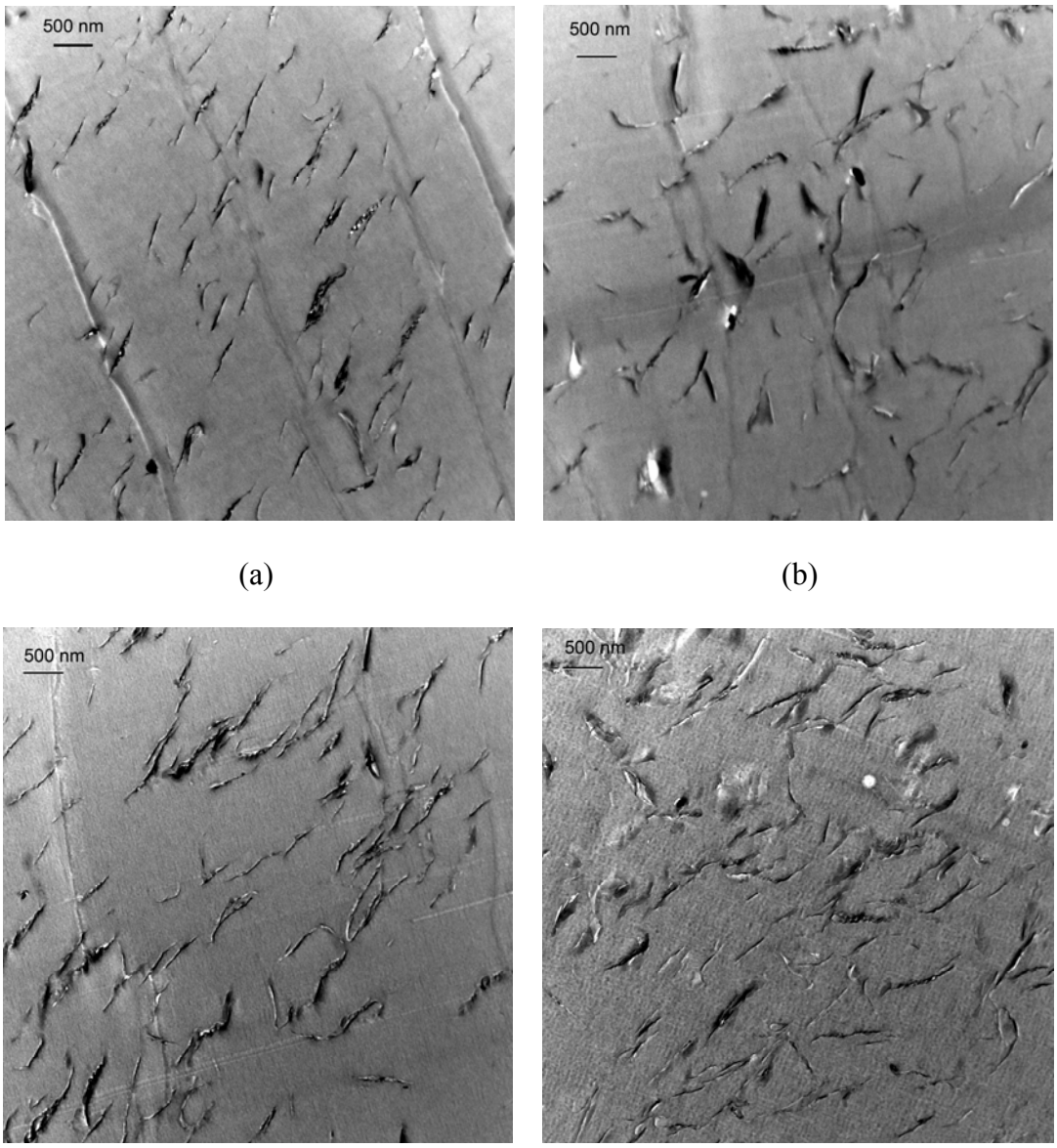

Figure 13: Temperature dependent TEM images of morphological evolution for PC16-MMT/PS nanocomposite (5% mass fraction) (a) room temperature; (b) 250 °C for 5 min; (c) 300 °C for 5 min (d) 350 °C for 5 min